Optical Materials 120 (2021) 111419

Contents lists available at ScienceDirect

Optical Materials

journal homepage: www.elsevier.com/locate/optmat

Research Article

Higher-performance Fabry-Perot microlaser enabled by a quadrilateral microwire via Ag nanowires decoration

Hongliang Dang [a], Xiangbo Zhou [a], Binghui Li [b,**], Caixia Kan [a], Mingming Jiang [a,*]

[a] College of Science, MIIT Key Laboratory of Aerospace Information Materials and Physics, Key Laboratory for Intelligent Nano Materials and Devices, Nanjing University of Aeronautics and Astronautics, No. 29 Jiangjun Road, Nanjing, 211106, PR China

[b] State Key Laboratory of Luminescence and Applications, Changchun Institute of Optics Fine Mechanics and Physics, Chinese Academy of Sciences, Changchun, 130033, PR China

ARTICLE INFO

Keywords:
Fabry-perot cavity
Lasing
ZnO microwire
Ultraviolet plasmons
Ag nanowire

ABSTRACT

In this work, ultraviolet Fabry-Perot (FP) microlaser, made of an individual rectangular-shaped ZnO microwire, was achieved. The bilateral smooth facets and single-crystalline specificity of as-grown ZnO microwires can enable the realizing of lateral FP microresonators. By incorporating Ag nanowires (AgNWs), plasmon-enhanced FP lasing performances of an individual ZnO microwire, specifically for the sharply reduced threshold, increased lasing intensity and increased *Q*-factor, were achieved. Accordingly, the enhanced working principle was implemented, and is resorting to the confinement and enhancement of localized electromagnetic-field produced by AgNWs, which can make up the metal loss and accelerate more radiative recombination. Thereby, the incorporation of a rectangular-shaped microwire and AgNWs via desired ultraviolet plasmons can be used to exploit the modulation of metal nanostructures on lasing characteristics of wide bandgap semiconductors. Further, this study also suggestes that AgNWs with excellent ultraviolet plasmons can be generally utilized to modulate the optoelectronic characteristics of wide bandgap semiconductor materials and devices, indicating its underlying applications in fabricating high-performance light-emitting diodes and lasers, photodetectors and so on, working in the ultraviolet wavelengths.

1. Introduction

Microsized laser devices have undergone breathtaking progress over the last few years and become a vital component in evolving coherent light sources, particularly the subminiaturized laser devices. That is, they can support excellent ability of optical confinement, and characterize expressly enhancing light-matter interactions [1–5]. The original microlasers design are mostly based on optical microresonators, containing whispering gallery mode (WGM) [6,7], Fabry-Perot (FP) modes [8,9], photonic crystal modes [10,11] and distributed feedback (DFB) modes [12,13]. By comparison, one of the most distinct characteristics arising from the FP microcavities, like output directionality, can be developed for knowledgeable applications. The perspective of designing and constructing creative FP resonators, and the corresponding FP-like laser devices has drawn growing interest [8,14–16]. Among the configurations of fabricating optical microcavities, nanowires (NWs) can naturally form FP microcavities with two end-facets working as reflecting mirrors. That is, light is confined inside wires and oscillates between two end-facets [17–19]. However, increasing the large axial length of low-dimensional semiconductors, the micro/nanowire lasers representatively exhibit multimode lasings, which greatly influences the corresponding lasing threshold, the output color purity, directionality and temporal stability [20–22].

As increasing the cross-sectional size of one-dimensional wires, specifically for the diameter, the electromagnetic wave can be confined in the cross section, wherein the light resonances are satisfied with a closed round trip of the oscillating modes. That is, the light is totally reflected at the inwall facets of low-dimensional micro- and nanostructures. This kind of electromagnetic field confinement and localization for the light wave within the inwalls via total internal reflection have been extensively employed to fabricating WGM microresonators [23–25]. Apart from the WGM cavities, another light oscillation between two opposing parallel facets serving as highly reflective mirrors can also be observed, like FP microresonators [26–28]. Recently,

* Corresponding author.
** Corresponding author.
E-mail addresses: binghuili@163.com (B. Li), mmjiang@nuaa.edu.cn (M. Jiang).

https://doi.org/10.1016/j.optmat.2021.111419
Received 2 April 2021; Received in revised form 17 July 2021; Accepted 25 July 2021
Available online 30 July 2021

semiconductor micro/nanostructures with rectangular-shaped cross section, such as nano-/microcubes, microwires (MWs) and microribbons, have been employed to construct FP microcavities, which being implementated by the light oscillation between the lateral facets of semiconductor microcrystals [14,26,28,29]. ZnO is a typical semiconductor having a broad bandgap and high energy of exciton binding, that makes it interesting for many electronic and optical applications in the ultraviolet wavelengths. Nowadays, ZnO micro-/nanostructures, like microrods, microribbons, microdisks and so forth, have been prepared successfully through hydrothermal synthesis, chemical vapor deposition (CVD), metal-organic vapor phase epitaxial technology, laser ablation and template-based synthesis [30–34]. Accordingly, the corresponding optical resonance modes of low-dimensional ZnO laser devices depend principally on their geometric morphology and intrinsic gain properties, yielding outstanding significances to design and fabricate optoelectronic devices [35–38]. Despite some accomplishments of ultraviolet lasing actions being achieved in ZnO-based NWs, MWs, microdisks, microrods, and nanoribbons etc., relevant studies in fabriating high-performance ultraviolet FP lasing behavior based on quadrilateral ZnO MWs are still in their infancy [39–43].

In the present study, individual ZnO MWs with quadrilateral morphology and straight side walls were obtained self-catalyzed by using CVD method. A new kind of microsized FP laser devices, composed of an individual quadrilateral ZnO MW, was realized upon ultraviolet pumping, and its operating behaviors was featured in the ultraviolet wavelengths. Due to high optical gain, the single ZnO MW can provide a workable platform to achieve FP lasing, which naturally enabled by the bilateral facets of the MW. By introducing Ag nanowires (AgNWs), the FP-mode lasing features was greatly improved, including the much lower threshold, higher *Q*-factor of FP-microresonantor, and the significantly enhanced lasing intensity. To exploit the enhanced working principle, the plasmonic response of AgNWs being excited by ultraviolet excitation can reorganize the surface electron wave at the surfaces of the ZnO MW, which efficiently reduce the optical loss, together with the improvement of light confinement and localization within the wire. The increased working principle was evidenced by means of time resolved photoluminescence (TRPL) characterization and finite different time domain (FDTD) simulation. This study can deepen and promote its further research and application in developing high-performance microsized semiconductor coherent light sources and photodetectors operating in the ultraviolet wavelengths.

2. Results and discussion

It is widely reported, individual ZnO MWs with well-defined crystallographic facets have been prepared. To achieve the MWs with quadrilateral cross-section, the growth conditions, particularly for the oxygen-deficient environment, should be regarded with great attention [28,38]. The as-synthesized samples were measured using a scanning electron microscope (SEM). Illustration of a SEM image in Fig. 1(a) exhibits that an individual ZnO MW possesses well-constructed smooth surfaces, and the width of the wire is evaluated to about 10 μm. The crystal character of ZnO MWs was characterize by X-ray diffraction (XRD) analysis. As demonstrated in Fig. 1(b), the XRD patterns of the samples exhibits the presence of wurtzite ZnO phase (JCPDS 65–3411), and the corresponding cell constants is extracted of a = 3.24 $\dot{A}$ and c = 5.19 $\dot{A}$ [7]. AgNWs were prepared by the slow injection polyvinylpyrrolidone (PVP)-directed polyol method [44,45]. By using spin-coating technique, an individual ZnO MW covered by AgNWs (AgNWs@ZnO), was fabricated as follows [44,46]. First, a ZnO MW was placed on quartz substrate. Second, the solution of AgNW via certain concentration was deposited on the entire wire, and then followed by a thermal annealing (the temperature at 100 °C), leading to a preparation of an individual AgNWs@ZnO MW. Varying the volume of the AgNWs droplets, the coverage concentration of AgNWs can be easily modulated [28,44,47]. Fig. 1(c) demonstrates SEM image of a ZnO MW covered by AgNWs. It is obviously illustrated that AgNWs with uniform distribution can be deposited on ZnO MWs.

The as-synthesized AgNWs was characterized. SEM image displayed in Fig. 1(d), exhibits an average diameter ~ 50 nm and average length ~

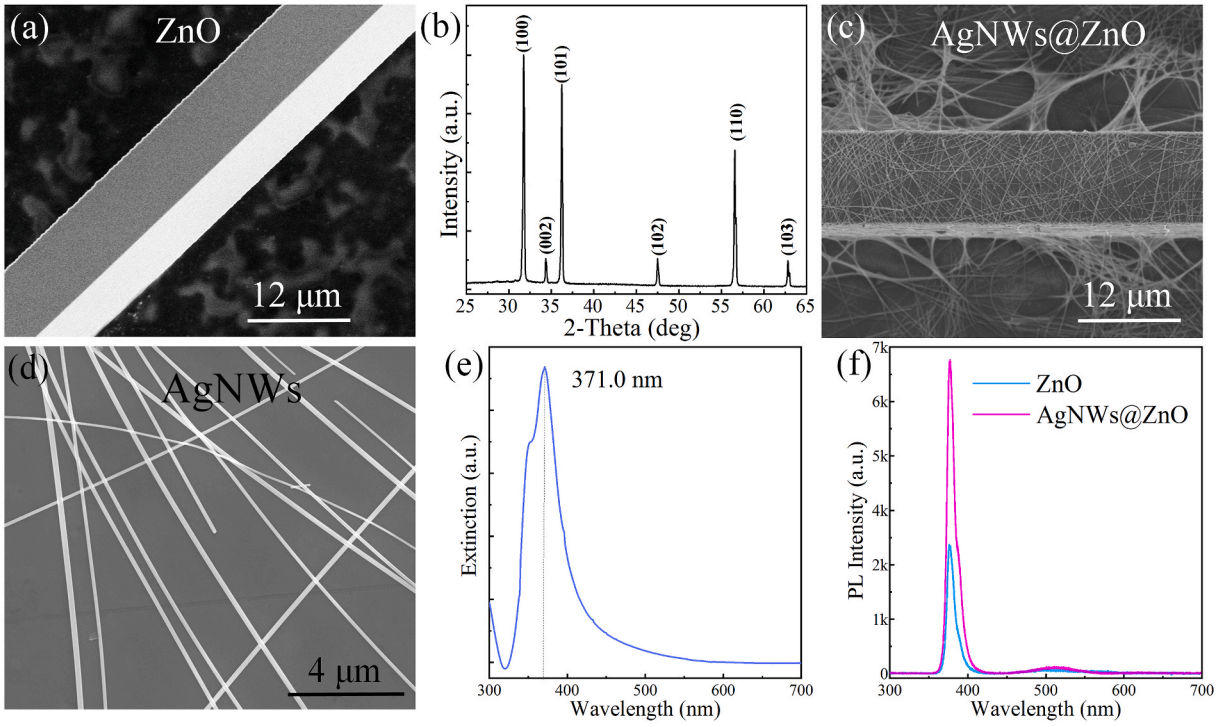

Fig. 1. (a) SEM image of an individual ZnO MW. (b) XRD peaks of the as-synthesized ZnO MWs. (c) SEM image of a ZnO MW covered by AgNWs. (d) SEM image of as-synthesized AgNWs, with the diameter of about 50 nm. (e) Extinction spectrum of the as-synthesized AgNWs, and the main extinction peak positioned at around 371.0 nm. (f) PL spectra of a ZnO MW not decorated, and decorated by AgNWs.

10 μm. Accordingly, the optical extinction of these AgNWs was measured by using a UV-6300 spectrophotometer. The main wavelength in the extinction peak was obtained at about 371 nm, as demonstrated in Fig. 1(e). To exploit the influence of AgNWs on the optical properties, photoluminescence (PL) measurements of ZnO MW not covered, and covered by AgNWs, were performed by using a He–Cd laser via a LABRAM-UV Jobin Yvon spectrometer (the pumping wavelength at 325 nm). Upon ultraviolet excitation, the emitted photons were recorded, and the optical spectrum was plotted in Fig. 1(f). It exhibits that the main wavelength of PL spectrum of single bare ZnO MW is observed at 380.0 nm, operating in the ultraviolet band. The unique ultraviolet PL emission is assigned to typical near-band-edge (NBE) emission of ZnO [7,29]. Additionally, the other negligible broadband visible radiation, could be attributed to the intrinsic defect related luminescence. Conclusively, the as-synthesized samples show superior crystalline quality [7,28]. Interestingly, by introducing the AgNWs, an observably increased ultraviolet emission of the ZnO MW was acquired. The improved character can be interpreted as the interaction of ZnO excitons coupled with localized plasmons of the deposited AgNWs [28,39,48].

As we all known that, semiconductor microcrystals with smooth facets can potentially feature as the reflecting mirrors for designing and engineering optical microresonators. Combining with the outstanding lasing gain of ZnO, it is highly workable to design lateral-cavity FP microlaser based on an individual quadrilateral ZnO MW. Schematic of the optically pumped a quadrilateral ZnO MW based FP microlaser was demonstrated in Fig. 2(a). Shown in the device architecture, the utilizing single ZnO MW with quadrilateral cross section naturally form a FP microresonator, with both the bilateral sides functioning as reflecting mirrors. Thereby, light can be confined inside the MW, and oscillate between two bilateral facets. Taken a single quadrilateral MW shown in Fig. 2(b) for example, the SEM image exhibits a perfect quadrilateral, cylindrical structure, whilst smooth side surfaces. To confirm the self-constructed FP cavity, theoretical simulation of standing-wave field distribution via FP resonant modes in the rectangular-shaped cross section of the wire were checked by utilizing FDTD method [28,41]. In the calculation, perfect matched layer (PML) was adopted to absorb the outgoing waves. A single ZnO MW with quadrilateral cross-section placed on a quartz substrate was modeled. The width of the MW is set to $D = 10$ μm, the incident wavelength λ is 390 nm; the refractive indexes of ZnO n_{ZnO}, quartz substrate n_{quartz} and air n_{air} are set to 2.35, 1.5 and 1.0, respectively. As shown in Fig. 2(c), FP oscillation created in the quadrilateral cross section of ZnO MW was well simulated numerically, thus, both the lateral sides can serve as the reflecting mirrors [14,30,41]. Further, the enlarged electric-field distributions at the air/ZnO interface were extracted, and demonstrated in Fig. 2(d)–(f). The oscillating feedback in the bilateral microresonator can be evidenced by the periodically distribution of antinodes and nodes of simulated electromagnetic fields, which observably acknowledged by the resonant patterns.

To confirm the FP character, a ZnO MW was optically pumped by using a fs pulsed laser consisting of an optical parametric amplifier (OPERA SOLO) with a Ti:sapphire laser (coherent) and a confocal micro-PL system (Olympus BX53). The radiated photons were collected by using a spectrometer (SpectraPro-2500i, Acton Research Corporation) [7,28,49]. Upon the ultraviolet excitation, optical PL image with an observable luminescence area can be captured. It indicates that the single ZnO MW can emit a powerful beam of light, with luminescence regions distributed at the bilateral edges of the wire. To study the luminescence modes, it may be assigned to the specific FP. That is, both the lateral facets can be used for the reflection mirrors featuring the total internal reflection. Varying the pump fluence, Fig. 3(a) shows PL spectra of a single ZnO MW. As the pumping fluence increased less than 2.98 mJ/cm^2, the obtained PL spectra are dominated by spontaneous luminescences. The main wavelengths of PL situates at around 383.0 nm, and spectral linewidth of about 12 nm. As the excitation fluence reaches 3.25 mJ/cm^2, a group of sharp spikes with evenly mode spacing can be observed. Above all, the increase of light intensity as a function of the excitation power exhibits a nonlinear feature. The experimental results indicate that the lasing action of an individual quadrilateral ZnO MW upon ultraviolet pumping may be attributed to FP.

As the excitation fluence increased above 3.25 mJ/cm^2, the PL spectra are completely governed by a series of sharp luminescence peaks, and the sharp peak intensity increases sharply. These may be

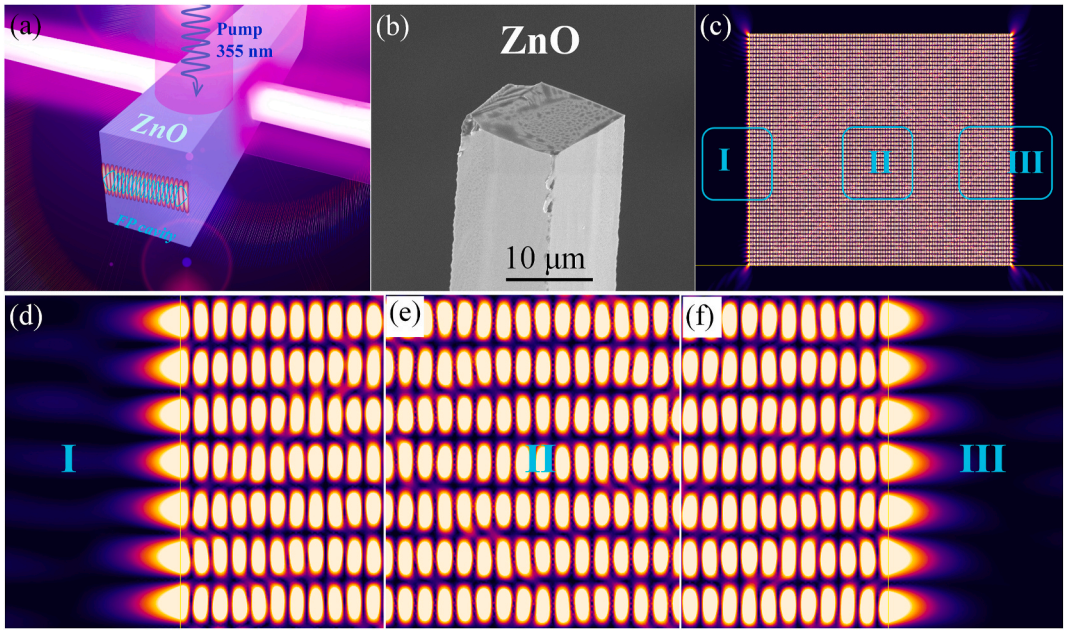

Fig. 2. (a) Schematic representation of the lasing experiments for FP-mode microlaser device involving a ZnO MW with quadrilateral cross section, which pumped by ultraviolet excitation via fs pulsed laser (the pumping wavelength of 355 nm). (b) SEM image of ZnO MW via the quadrilateral cross-section. (c) Cross-sectional plots of the electric-field distribution $|\mathbf{E}|^2$ inside the lateral cavity, which naturally formed by the bilateral facets of a quadrilateral ZnO MW. In the figure, three different regions were labelled as **I**, **II** and **III**, respectively. Enlarged electric-field intensities at the interface of ZnO/Air (d) region-**I**, (e) region-**II** inside the wire, and (f) the region-**III**, respectively.

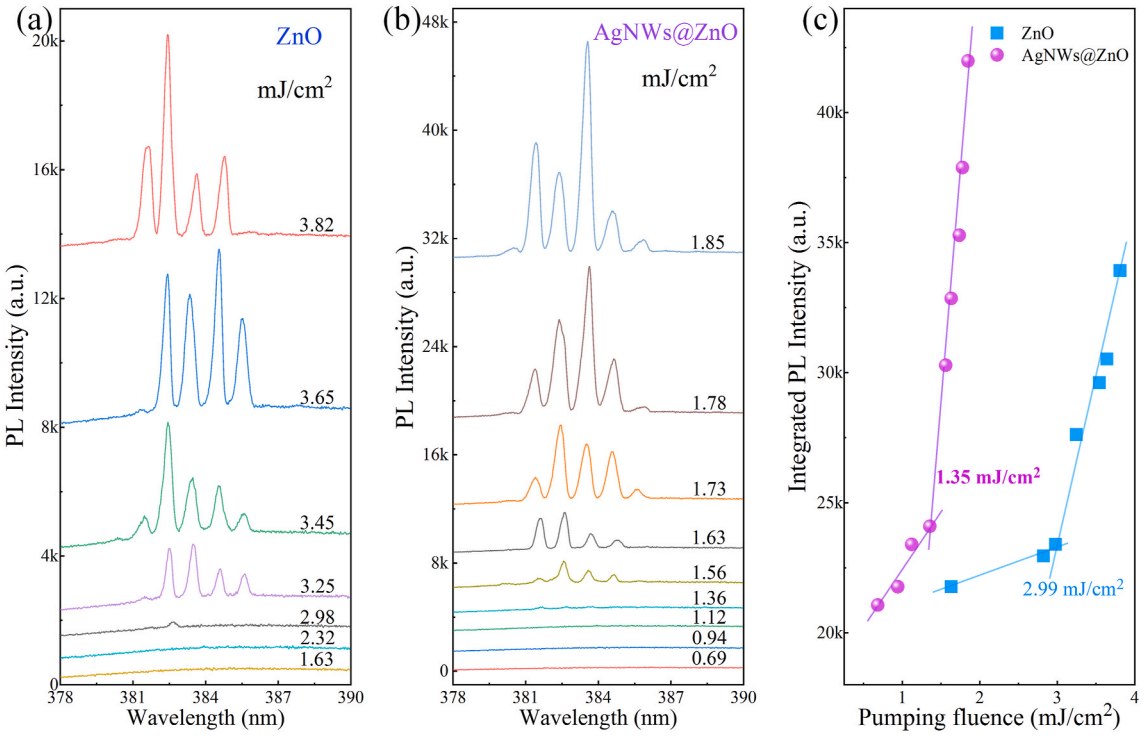

Fig. 3. FP lasing characterization of a ZnO MW not decorated, and decorated by AgNWs. Under ultraviolet excitation via a fs pulsed laser, PL spectra of the single ZnO MW not covered (a), and covered by AgNWs (b), as functions of the pumping fluence. (c) Integrated PL intensity versus the pumping fluence of the ZnO MW not covered, and covered by AgNWs.

explained through the amplification of FP mode by the optical feedback in the quadrilateral cross section of ZnO MW. Regardless of the excitation fluence, the peak spacing between nearby oscillation mode, is seemingly constant. Taken a pumping fluence of 3.65 mJ/cm^2 for instance, multimode peaks with uniformly spaced gap ($\Delta\lambda$) is extracted to be 1.20 nm, and full width at half maximum (FWHM) ($\delta\lambda$) is evaluated to be 0.38 nm. Thereby, the Q-factor is evaluated to about 1000 due to the formula of $Q = \lambda/\delta\lambda$, where λ is the peak wavelength. Further, theoretical analysis on the PL emission feature of the single ZnO MW was performed. The formula of the mode spacing for FP-type optical cavity [14,26,38,41],

$$\Delta\lambda = \frac{\lambda^2}{2L_c\left(n - \lambda\frac{dn}{d\lambda}\right)}, \quad (1)$$

where L_c is the width of the quadrilateral cross-section of the wire, $dn/d\lambda = -0.010$ nm^{-1} at 390 nm [14,38]. The cavity length L_c is evaluated to about 10 μm, which is approximatively agreed with the experimentally observed value. Therefore, ZnO MWs with quadrilateral morphologies and straight facets can be used to developing FP microlasers.

Contrast that with a hexagonal ZnO MW via the approximate size (the diameter of hexagon-shaped MW is equal to the width of the wire with quadrilateral cross-section), optically pumped FP lasing characteristics of the quadrilateral ZnO MW exhibit relatively higher threshold, and much lower Q-factor [7,39,41]. Fortunately, nanostructured metals having outstanding plasmonic response, can be utilized to improving the lasing performances, such as the enhanced luminescence efficiency, the increased Q-factor and the reduced threshold [39,50]. In recent years, noble metals containing Ag, Al, and Ga, are currently featured as ultraviolet plasmonic materials because of their unique responses in the shorter wavelengths [39,51,52]. Exploring nanostructured metals with regard to their plasmonic behaviors, including high stability against various complicated environments, the controlled sizes, and energy-tunable plasmons in the ultraviolet wavelengths, is ongoing [43,46,53].

Being generally worked as ultraviolet plasmonic materials, AgNWs were successfully synthesized [45,48]. The nanostructured Ag can produce spatially localized electromagnetic field, and can highly increase enhanced characteristics of optical field around the sharp tips. The unique plasmonic influence can efficiently increase the optical performances of low-dimensional ZnO nano/microcrystals [28,39,54]. To study the influence of AgNWs on the FP lasing features, the same ZnO MW covered by AgNWs were also illuminated by a fs laser. Fig. 3(b) represents luminescence spectra by varying the pump power. As the pumping fluence reaches 1.56 mJ/cm^2, a group of sharp peaks appeared in the spontaneous emission background, can be captured. Thus, the incorporation of AgNWs can contribute FP-lasing action because of selectively amplified by the enhanced optical feedback in the cavity self-constructed by the AgNWs@ZnO MW. Compared with that of the bare ZnO MW, the Q-facor is increased up to about 1300. Additionally, the integrated light intensity in terms of excitation energy was plotted in Fig. 3(c). Shown in the figure, the lasing threshold P_{th} of the AgNWs@ZnO MW was extracted to be about 1.33 mJ/cm^2, which much lower than that of the same bare MW. Therefore, the reduced threshold and increased lasing intensity of the AgNWs@ZnO MW based microlaser indicates that the ultraviolet plasmons of AgNWs can be utilized to improve the performance of the FP microcavity [27,28,39].

Illustration in Fig. 4(a), PL spectrum of the bare ZnO MW at the pumping fluence of 3.25 mJ/cm^2, exhibits that the mode spacing $\Delta\lambda$ is extracted to about 1.20 nm, the FWHM $\delta\lambda$ is extracted to about 0.38 nm. Accordingly, the Q-factor is evaluated to about 1000. The corresponding bright-field optical PL image from the bare ZnO MW was captured in Fig. 4(c). Clearly, bright lighting spots was recorded, and the luminescence regions distribute along the two lateral facets of the rectangular-shaped wire. It indicates that strong waveguide oscillating along the width of the wire, can enable the fabricating lateral FP microresonator. Further, the modulation of AgNWs on the luminescence features of the quadrilateral ZnO MW was made. The lasing spectra from the MW not decorated, and decorated by AgNWs, which being illuminated at the

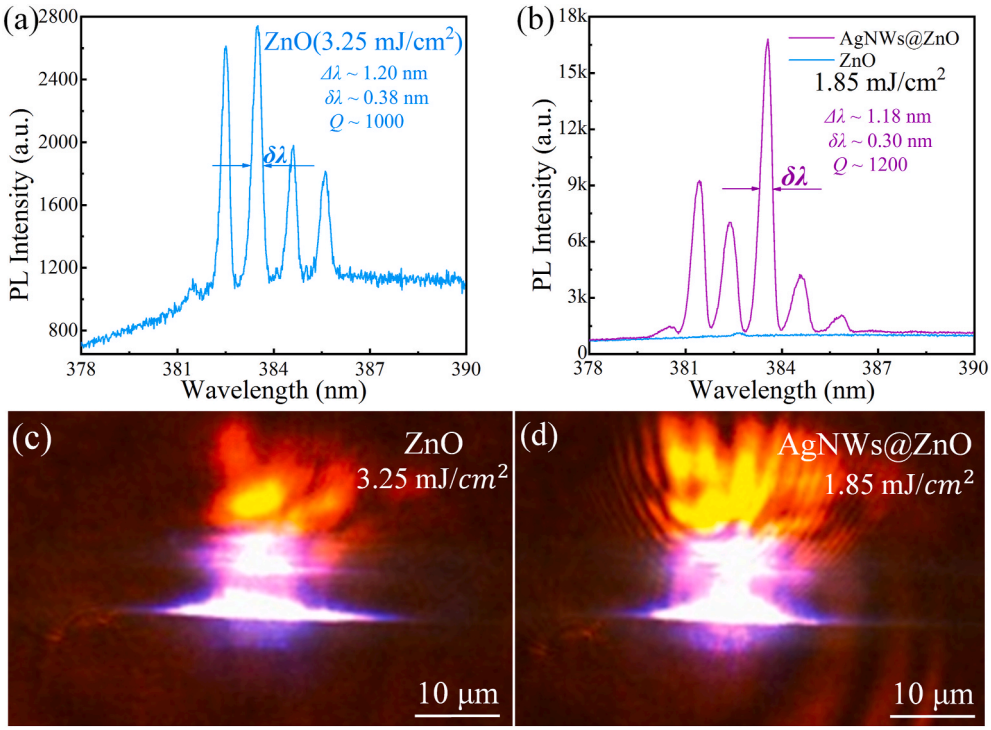

Fig. 4. (a) PL spectrum of a bare ZnO MW at a pumping power density of 3.25 mJ/cm^2. (b) Comparison of PL spectra of the ZnO MW not covered, and covered by AgNWs, at a pumping power density of 1.85 mJ/cm^2. (c) Optical microscope image of the bare ZnO MW under a pump fluence of 3.25 mJ/cm^2. (d) Optical microscope image of the same ZnO MW covered by AgNWs under a pump fluence of 1.85 mJ/cm^2.

same excitation power intensity of 1.85 mJ/cm^2, was plotted in Fig. 4 (b). It demonstrate that more than 15 times increased ratio of light intensity was acquired by introducing AgNWs on the ZnO MW. The corresponding bright-field PL image from the ZnO MW coated by AgNWs illustrates that much brighter dazzling light can radiate from both the bilateral sides of the MW, as illustrated in Fig. 4(d). In addition to the sharply reduced lasing threshold and remarkable increase of the light output, the *Q*-factor was obviously improved. Therefore, the FP lasing performance of the single quadrilateral ZnO MW was significantly enhanced through incorporating AgNWs on the wire.

As we described above, the achievement of plasmons-mediated FP lasing properties of single ZnO MW is realized by introducing AgNWs with desired ultraviolet plasmonic response. To exploit the enhanced working principle of AgNWs on the FP lasing properties of the single ZnO MW, the time-resolved photoluminescence (TRPL) measurement was performed by using an optically triggered streak camera system (C10910, Hamamatsu) at 295 nm through frequency-doubling of the fundamental 35-fs pulses at 590 nm with a repetition rate of 1 kHz (OperA Solo, Coherent) [28,39,41]. The tested TRPL results from single ZnO MW not decorated, and decorated by AgNWs, are shown in Fig. 5 (a). According to the fitted TRPL decay curves, the luminescence lifetime of the ZnO MW decorated by AgNWs ~ 177.7 ps is observable shorter than that of the bare wire (~ 276.9 ps). Further, temporal spectroscopic profiles of the bare ZnO MW, and the MW decorated by AgNWs, were further exhibited in Fig. 5(b) and (c), respectively. Compared with bare MW, a much faster decay rate of the AgNWs-decoated ZnO MW can be achieved. The carrier lifetime of ZnO MWs is observably reduced by coating AgNWs layer. That is, the incorporation of the AgNWs can successfully facilitate the carrier recombination of ZnO excitons. By compared with that of the bare ZnO MW, a new path of carrier recombination could be emerged. Due to the TRPL studies, it can be deduced that AgNWs-plasmon can efficiently couple with ZnO excitons [39,48,54].

Moreover, the role of AgNWs plasmons and the underlying enhanced mechanism in fabricating high-efficiency low-dimensional laser devices working in the ultraviolet wavelengths were implemented. Numerical calculations of FP cavity and near-field electromagnetic responses of a single AgNW, which deposited on ZnO MW, were performed via FDTD method [28,39,41]. In the simulation, an individual AgNW was modeled using pentagon-shaped wire, according to the SEM image of AgNWs, which shown in Fig. 5(d) (The cross section of an individual AgNW exhibits pentahedron-shaped morphology). A ZnO MW covered with AgNWs were built up (the width of quadrilateral ZnO MW $D = 10.0\ \mu$m). The calculated parameters are supplied, including refractive indexes of ZnO MW ($n_{ZnO} = 2.35$), quartz substrate ($n_{SiO_2} = 1.5$), air ($n_{air} = 1$). The incident light termed as propagating plane wave, was illuminated at the model, leading to interacte with the target (the excitation wavelength at 370 nm). The spatially localized electric-field intensity distribution of an individual AgNW was calculated numerically. It can be obviously seen that the calculated near-field are mainly concentrated at the endpoints of pentagon-shaped cross section from the simulated optical path along the *x*-direction (Fig. 5(e)) and *y*-direction (Fig. 5(f)) in the *x*-*y*-plane. Thus, the strongest enhancement of localized electromagnetic field can occur at the sharp tips of the pentagon-shaped AgNW [28,44,55].

The spatially localized electric-field intensity distribution of an individual AgNW placed on ZnO MW was also calculated numerically. As illustrated in Fig. 5(g), significantly increased electromagnetic field can be observed at the AgNWs/ZnO interface from the optical path along *x*-*z*-plane. The enhanced confinement and localization of the simulated fields can be ascribed to the excitation of localized surface plasmons of AgNWs. In the hybrid architecture, AgNWs can work as plasmonic antennas, resulting in strong interacting with the incident light. The nanostructured metals can concentrate the incident electromagnetic energy localized at the AgNWs/ZnO interface, and then interacted with the ZnO excitons availably [28,44]. From these simulated results, it is observably illustrated that the light wave propagating horizontally in the quadrilateral wires was dramatically intensified due to the increasing reflections at the AgNWs@ZnO/air boundary. And it also indicates that the performance of a single-ZnO-MW enabled FP microresonator is improved by depositing AgNWs. Incorporated with the

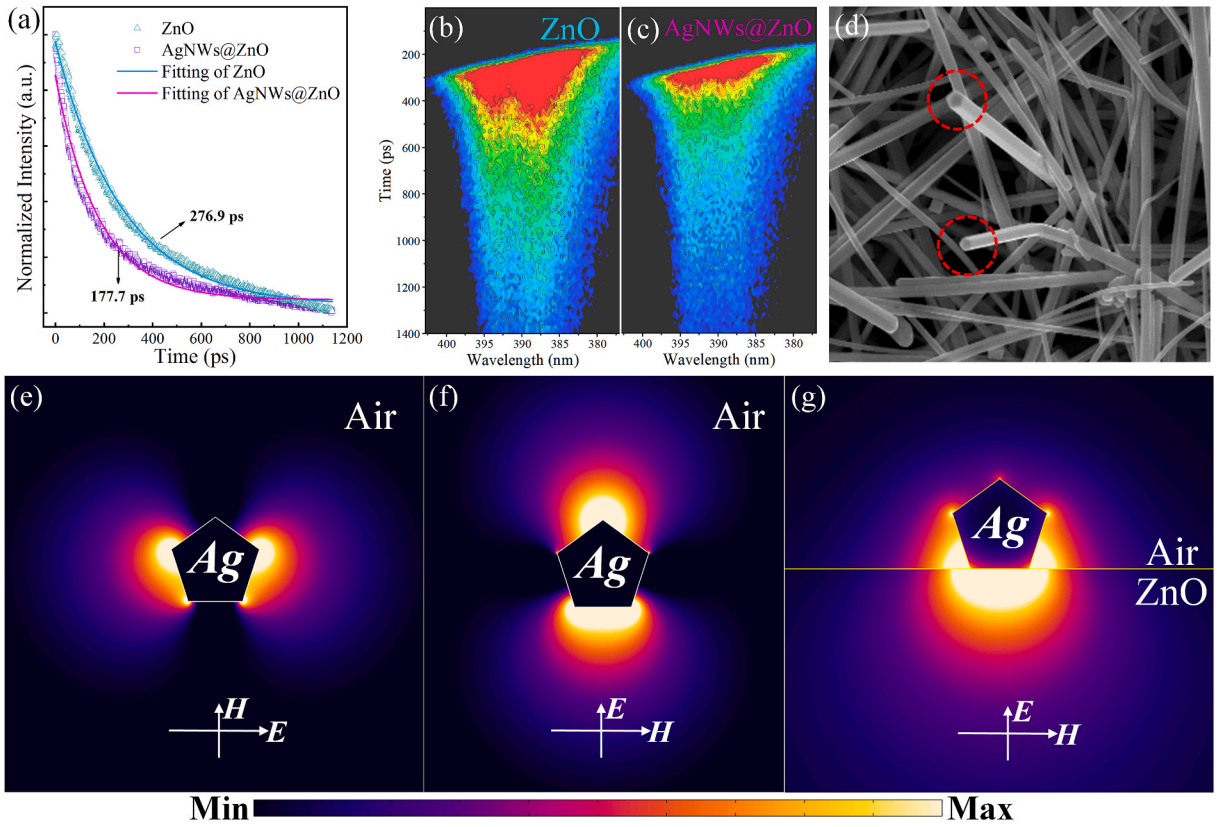

Fig. 5. (a) Time-resolved PL signals (dots) and fitted curves (solid lines) illustrate a decay time of 276.9 ps for the bare ZnO MW; by depositing AgNWs, the decay time reduced to about 177.7 ps for the same ZnO MW. (b) Temporal spectroscopic profile of (b) the bare ZnO MW, and (c) the AgNWs-coated ZnO MW. In the measurement, the samples were excited by 295 nm laser, and the light signals were collected by a streak camera. (d) SEM image of the as-synthesized AgNWs, illustrating pentagon-shaped cross section (the red dotted line). The diameter of a AgMW is about 50 nm. The electric field distributions of a pentagon-shape AgNW at the wavelength of 370.0 nm (e) and (f) for the different incident **E**-direction. (g) Electric-field intensity distribution at the *x*-*z* plane of the cross section along the AgNW/ZnO interface. In the simulation, the incident light is illuminated normally from above and polarized in the *x*-*z* plane.

near-field localization and enhancement of AgNWs, it can be concluded that plasmonic energies generated from AgNWs-plasmon can permeate into the neighboring ZnO MW, reorganizing the localized optical-field distribution. It suggestes that ultraviolet plasmonic response of AgNWs can be utilized to increasing the lasing properties of individual ZnO MWs based microlaser devices [39,41,44].

3. Conclusions

To summarize, lateral-cavity supported FP microlasers from individual quadrilateral ZnO MWs were demonstrated. The current lateral cavity microlaser outputs from both the bilateral sides of the MWs. Perhaps in future, the coating of totally reflecting mirror on one facet of the quadrilateral MW, may lead to realizing unidirectional coherent output. More significantly, AgNWs serving as broadly used ultraviolet plasmonic antennas, were utilized to advance FP lasing properties of an individual ZnO MW. By incorporating AgNWs, improved FP lasing characteristics, containing the sharply reduced threshold and increased *Q*-quality, were observably reached. The excitation of AgNWs plasmons towards the interface of AgNWs/ZnO can reorganize the localized electromagnetic field, such as compensating the optical loss, and accelerating more photons confined in the FP microresonators, which naturally created by the bilateral facets of the quadrilateral microstructures. The representative results are significative, not only to interpretate the coupling between nanostructured metals and semiconductors in physics, but also to motivate innovative design of plasmons-mediated high-performance optoelectronic devices in technology. We expect that achieving high-performance lateral-cavity FP lasers in microsized level can contribute to the broadest applications in fabricating highly integrated coherent light sources.

CRediT authorship contribution statement

Hongliang Dang: Conceptualization, Synthesis of ZnO MWs, AgNWs and Structural Characterizations, Device Characterizations, Writing-Original draft preparation, Writing – original draft. **Xiangbo Zhou:** Synthesis of ZnO MWs, AgNWs and Structural Characterizations, Device Characterizations. **Binghui Li:** Conceptualization, Writing- Reviewing . **Caixia Kan:** Conceptualization, Writing- Reviewing and Editing, Writing – review & editing. **Mingming Jiang:** Editing, Writing – review & editing, Conceptualization, Synthesis of ZnO MWs, RhNCs and Structural Characterizations, Device Characterizations, Writing-Reviewing and Editing, Writing – review & editing.

Declaration of competing interest

The authors declare that they have no known competing financial interests or personal relationships that could have appeared to influence the work reported in this paper.

Acknowledgements

This work was supported by the National Natural Science Foundation of China (Grant Nos. 11974182, U1604263, 11774171, 21805137 and 11874220), the Fundamental Research Funds for the Central Universities (No. NT2020019), Open Fund of Key Laboratory for Intelligent Nano Materials and Devices of the Ministry of Education (No. INMD-2020M03).

References

[1] A. Graf, M. Held, Y. Zakharko, L. Tropf, M.C. Gather, J. Zaumseil, Electrical pumping and tuning of exciton-polaritons in carbon nanotube microcavities, Nat. Mater. 16 (2017) 911–917.

[2] X. Yu, Y. Yuan, J. Xu, K.-T. Yong, J. Qu, J. Song, Strong coupling in microcavity structures: principle, design, and practical application, Laser Photon. Rev. 13 (1) (2019) 1800219.

[3] Q. Shang, S. Zhang, Z. Liu, J. Chen, P. Yang, C. Li, W. Li, Y. Zhang, Q. Xiong, X. Liu, Q. Zhang, Surface plasmon enhanced strong exciton-photon coupling in hybrid inorganic-organic perovskite nanowires, Nano Lett. 18 (6) (2018) 3335–3343.

[4] D. Yan, T. Shi, Z. Zang, S. Zhao, J. Du, Y. Leng, Stable and low-threshold whispering-gallery-mode lasing from modified CsPbBr3 perovskite quantum dots@ SiO2 sphere, Chem. Eng. J. 401 (2020) 126066.

[5] O. Jamadi, F. Reveret, P. Disseix, F. Medard, J. Leymarie, A. Moreau, D. Solnyshkov, C. Deparis, M. Leroux, E. Cambril, S. Bouchoule, J. Zuniga-Perez, G. Malpuech, Edge-emitting polariton laser and amplifier based on a ZnO waveguide, Light, Sci. Appl. 7 (1) (2018) 82.

[6] N. Toropov, G. Cabello, M.P. Serrano, R.R. Gutha, M. Rafti, F. Vollmer, Review of biosensing with whispering-gallery mode lasers, Light Sci. Appl. 10 (8) (2021) 42.

[7] C. Xu, J. Dai, G. Zhu, G. Zhu, Y. Lin, J. Li, Z. Shi, Whispering-gallery mode lasing in ZnO microcavities, Laser Photon. Rev. 8 (4) (2014) 469–494.

[8] Q. Bao, W. Li, P. Xu, M. Zhang, D. Dai, P. Wang, X. Guo, L. Tong, On-chip single-mode CdS nanowire laser, Light: Sci. Appl. 9 (1) (2020) 42.

[9] N. Jukam, A wavelength-size tunable Fabry-Perot laser, Nature Photonics 13 (12) (2019) 823–825.

[10] H.-G. Park, S.-H. Kim, S.-H. Kwon, Y.-G. Ju, J.-K. Yang, J.-H. Baek, S.-B. Kim, Y.-H. Lee, Electrically driven single-cell photonic crystal laser, Science 305 (5689) (2004) 1444–1447.

[11] G. Marty, S. Combrie, F. Raineri, A. De Rossi, Photonic crystal optical parametric oscillator, Nat. Photonics 15 (2021) 53–58.

[12] O.V. Kozlov, Y.-S. Park, J. Roh, I. Fedin, T. Nakotte, V.I. Klimov, Sub–single-exciton lasing using charged quantum dots coupled to a distributed feedback cavity, Science 365 (6454) (2019) 672–675.

[13] Y. Zhang, Y. Yan, L. Yang, C. Xing, Y. Zeng, Y. Zhao, Y. Jiang, Ultraviolet luminescence enhancement of planar wide bandgap semiconductor film by a hybrid microsphere cavity/dual metallic nanoparticles sandwich structure, Opt. Express 27 (11) (2019) 15399–15412.

[14] Z. Wang, Y. Ren, Y. Wang, Z. Gu, X. Li, H. Sun, Lateral cavity enabled Fabry-Perot microlasers from all-inorganic perovskites, Appl. Phys. Lett. 115 (11) (2019) 111103.

[15] X. Yang, Z. Shan, Z. Luo, X. Hu, H. Liu, Q. Liu, Y. Zhang, X. Zhang, M. Shoaib, J. Qu, X. Yi, X. Wang, X. Zhu, Y. Liu, L. Liao, X. Wang, S. Chen, A. Pan, An electrically controlled wavelength-tunable nanoribbon laser, ACS Nano 14 (3) (2020) 3397–3404.

[16] Y. Zhong, Q. Wei, Z. Liu, Q. Shang, L. Zhao, R. Shao, Z. Zhang, J. Chen, W. Du, C. Shen, J. Zhang, Y. Zhang, P. Gao, G. Xing, X. Liu, Q. Zhang, Low threshold Fabry-Perot mode lasing from lead iodide trapezoidal nanoplatelets, Small 14 (35) (2018) 1801938.

[17] C. Zhao, M. Ebaid, H. Zhang, D. Priante, B. Janjua, D. Zhang, N. Wei, A. A. Alhamoud, M.K. Shakfa, T.K. Ng, B.S. Ooi, Quantified hole concentration in AlGaN nanowires for high-performance ultraviolet emitters, Nanoscale 10 (2018) 15980–15988.

[18] S. Chu, G. Wang, W. Zhou, Y. Lin, L. Chernyak, J. Zhao, J. Kong, L. Li, J. Ren, J. Liu, Electrically pumped waveguide lasing from ZnO nanowires, Nat. Nanotechnol. 6 (8) (2011) 506–510.

[19] Y. Wu, Y. Ren, A. Chen, Z. Chen, Y. Liang, J. Li, G. Lou, H. Zhu, X. Gui, S. Wang, Z. Tang, A one-dimensional random laser based on artificial high-index contrast scatterers, Nanoscale 9 (2017) 6959–6964.

[20] S. Skalsky, Y. Zhang, J.A. Alanis, H.A. Fonseka, A.M. Sanchez, H. Liu, P. Parkinson, Heterostructure and Q-factor engineering for low-threshold and persistent nanowire lasing, Light: Sci. Appl. 9 (1) (2020) 43.

[21] Y. Xiao, C. Meng, P. Wang, Y. Ye, H. Yu, S. Wang, F. Gu, L. Dai, L. Tong, Single-nanowire single-mode laser, Nano Lett. 11 (3) (2011) 1122–1126.

[22] D. Zhao, W. Liu, G. Zhu, Y. Zhang, Y. Wang, W. Zhou, C. Xu, S. Xie, B. Zou, Surface plasmons promoted single-mode polariton lasing in a subwavelength ZnO nanowire, Nanomater. Energy 78 (2020) 105202.

[23] L. He, a. K. Ozdemir, L. Yang, Whispering gallery microcavity lasers, Laser Photon. Rev. 7 (1) (2013) 60–82.

[24] S. Yang, Y. Wang, H. Sun, Advances and prospects for whispering gallery mode microcavities, Adv. Opt. Mater 3 (9) (2015) 1136–1162.

[25] C. Tessarek, R. Roder, T. Michalsky, S. Geburt, H. Franke, R. Schmidt-Grund, M. Heilmann, B. Hoffmann, C. Ronning, M. Grundmann, S. Christiansen, Improving the optical properties of self-catalyzed gan microrods toward whispering gallery mode lasing, ACS Photonics 1 (10) (2014) 990–997.

[26] M. Ding, D. Zhao, B. Yao, E. Shulin, Z. Guo, L. Zhang, D. Shen, The ultraviolet laser from individual ZnO microwire with quadrate cross section, Opt Express 20 (13) (2012) 13657–13662.

[27] W. Ma, J. Lu, Z. Yang, D. Peng, F. Li, Y. Peng, Q. Chen, J. Sun, J. Xi, C. Pan, Crystal-orientation-related dynamic tuning of the lasing spectra of CdS nanobelts by piezoelectric polarization, ACS Nano 13 (5) (2019) 5049–5057.

[28] C. Miao, H. Xu, M. Jiang, J. Ji, C. Kan, Employing rhodium tripod stars for ultraviolet plasmon enhanced Fabry-Perot mode lasing, CrystEngComm 22 (2020) 5578–5586.

[29] D. Vanmaekelbergh, L.K. van Vugt, Zno nanowire lasers, Nanoscale 3 (2011) 2783–2800.

[30] Q. Zhu, F. Qin, J. Lu, Z. Zhu, Z. Shi, C. Xu, Dual-band fabry-perot lasing from single ZnO microbelt, Opt. Mater. 60 (2016) 366–372.

[31] W. Mao, M. Jiang, J. Ji, P. Wan, X. Zhou, C. Kan, Microcrystal modulated exciton-polariton emissions from single ZnO@ZnO: Ga microwire, Photon. Res. 8 (2) (2020) 175–185.

[32] Y. Yan, C. Xing, W. Liu, Q. Wang, C. Xu, Y. Jiang, Current-induced thermal tunneling electroluminescence via multiple donor-acceptor-pair recombination, J. Mater. Chem. C 9 (2021) 1174–1182.

[33] A. Pieniazek, H. Teisseyre, D. Jarosz, J. Suffczynski, B.S. Witkowski, S. Kret, M. Bockowski, A. Reszka, M. Godlewski, A. Kozanecki, B.J. Kowalski, Growth and optical properties of ZnO/Zn1-xMgxO quantum wells on zno microrods, Nanoscale 11 (2019) 2275–2281.

[34] Q. Liu, T. Yasui, K. Nagashima, T. Yanagida, M. Hara, M. Horiuchi, Z. Zhu, H. Takahashi, T. Shimada, A. Arima, Y. Baba, Ammonia-induced seed layer transformations in a hydrothermal growth process of ZnO nanowires, J. Phys. Chem. C 124 (37) (2020) 20563–20568.

[35] X. Yang, C.-X. Shan, P.-N. Ni, M.-M. Jiang, A.-Q. Chen, H. Zhu, J.-H. Zang, Y.-J. Lu, D.-Z. Shen, Electrically driven lasers from van der Waals heterostructures, Nanoscale 10 (2018) 9602–9607.

[36] J. Dai, C.X. Xu, X.W. Sun, ZnO-microrod/p-GaN heterostructured whispering-gallery-mode microlaser diodes, Adv. Mater. 23 (35) (2011) 4115–4119.

[37] B. Zhao, F. Wang, H. Chen, L. Zheng, L. Su, D. Zhao, X. Fang, An ultrahigh responsivity (9.7 mA W-1) self-powered solar-blind photodetector based on individual ZnO-Ga2O3 heterostructures, Adv. Funct. Mater. 27 (17) (2017) 1700264.

[38] Z. Li, M. Jiang, Y. Sun, Z. Zhang, B. Li, H. Zhao, C. Shan, D. Shen, Electrically pumped Fabry-Perot microlasers from single Ga-doped ZnO microbelt based heterostructure diodes, Nanoscale 10 (2018) 18774–18785.

[39] C.X. Xu, F.F. Qin, Q.X. Zhu, J.F. Lu, Y.Y. Wang, J.T. Li, Y. Lin, Q.N. Cui, Z.L. Shi, A. G. Manohari, Plasmon-enhanced ZnO whispering-gallery mode lasing, Nano Res. 11 (6) (2018) 3050–3064.

[40] S.I. Azzam, A.V. Kildishev, R.-M. Ma, C.-Z. Ning, R. Oulton, V.M. Shalaev, M. I. Stockman, J.-L. Xu, X. Zhang, Ten years of spasers and plasmonic nanolasers, Light: Sci. Appl. 9 (2020) 90.

[41] J. Li, M. Jiang, C. Xu, Y. Wang, Y. Lin, J. Lu, Z. Shi, Plasmon coupled Fabry-Perot lasing enhancement in Graphene/ZnO hybrid microcavity, Sci. Rep. 5 (2015) 9263.

[42] K.G. Cognee, H.M. Doeleman, P. Lalanne, A.F. Koenderink, Cooperative interactions between nano-antennas in a high-Q cavity for unidirectional light sources, Light Sci. Appl. 8 (2019) 115.

[43] K.R. Son, B.R. Lee, M.H. Jang, H.C. Park, Y.H. Cho, T.G. Kim, Enhanced light emission from AlGaN/GaN multiple quantum wells using the localized surface plasmon effect by aluminum nanoring patterns, Photon. Res. 6 (1) (2018) 30–36.

[44] Y. Wu, J. Xu, M. Jiang, X. Zhou, P. Wan, C. Kan, Tailoring the electroluminescence of a single microwire based heterojunction diode using Ag nanowires deposition, CrystEngComm 22 (2020) 2227–2237.

[45] X. Zhu, J. Xu, F. Qin, Z. Yan, A. Guo, C. Kan, Highly efficient and stable transparent electromagnetic interference shielding films based on silver nanowires, Nanoscale 12 (2020) 14589–14597.

[46] L. Yang, Y. Wang, H. Xu, W. Liu, C. Zhang, C. Wang, Z. Wang, J. Ma, Y. Liu, Color-tunable ZnO/GaN heterojunction LEDs achieved by coupling with Ag nanowire surface plasmons, ACS Appl. Mater. Interfaces 10 (18) (2018) 15812–15819.

[47] Z. Sun, M. Jiang, W. Mao, C. Kan, C. Shan, D. Shen, Nonequilibrium hot-electron-induced wavelength-tunable incandescent-type light sources, Photon. Res. 8 (1) (2020) 91–102.

[48] C. Kan, Y. Wu, J. Xu, P. Wan, M. Jiang, Plasmon-enhanced strong exciton-polariton coupling in single microwire-based heterojunction light-emitting diodes, Opt. Express 29 (2) (2021) 1023–1036.

[49] K. Tang, M. Jiang, P. Wan, C. Kan, Continuous-wave operation of an electrically pumped single microribbon based Fabry-Perot microlaser, Opt. Express 29 (2) (2021) 983–995.

[50] Y. Wang, F. Qin, J. Lu, J. Li, Z. Zhu, Q. Zhu, Z. Ye, Z. Shi, C. Xu, Plasmon enhancement for vernier coupled single-mode lasing from ZnO/Pt hybrid microcavities, Nano Res. 10 (10) (2018) 3447–3456.

[51] B.D. Clark, C.R. Jacobson, M. Lou, J. Yang, L. Zhou, S. Gottheim, C.J. DeSantis, P. Nordlander, N.J. Halas, Aluminum nanorods, Nano Lett. 18 (2) (2018) 1234–1240.

[52] G.V. Naik, V.M. Shalaev, A. Boltasseva, Alternative plasmonic materials: beyond gold and silver, Adv. Mater. 25 (24) (2013) 3264–3294.

[53] S. Chen, X. Pan, H. He, W. Chen, J. Huang, B. Lu, Z. Ye, Enhanced internal quantum efficiency in non-polar ZnO/Zn0.81Mg0.19O multiple quantum wells by Pt surface plasmons coupling, Opt. Lett. 40 (15) (2015) 3639–3642.

[54] H. Li, J.-H. Li, K.-B. Hong, M.-W. Yu, Y.-C. Chung, C.-Y. Hsu, J.-H. Yang, C.-W. Cheng, Z.-T. Huang, K.-P. Chen, T.-R. Lin, S. Gwo, T.-C. Lu, Plasmonic nanolasers enhanced by hybrid graphene-insulator-metal structures, Nano Lett. 19 (8) (2019) 5017–5024.

[55] S. Nauert, A. Paul, Y.-R. Zhen, D. Solis, L. Vigderman, W.-S. Chang, E.R. Zubarev, P. Nordlander, S. Link, Influence of cross sectional geometry on surface plasmon polariton propagation in gold nanowires, ACS Nano 8 (1) (2014) 572–580.